EFFECTS OF THE NMDA-R ANTAGONIST, MK-801, ON THE SEPTO-HIPPOCAMPAL NETWORK FUNCTIONAL CONNECTIVITY

By

Erik Hakopian
A capstone project submitted for Graduation with University Honors

May 09, 2024

University Honors
University of California, Riverside

APPROVED

Dr. Vasileios Christopoulos
Department of Bioengineering

Dr. Richard Cardullo, Howard H Hays Jr. Chair
University Honors

ABSTRACT

The N-methyl-d-aspartate receptor (NMDAR) hypofunction hypothesis has been proposed to help understand the etiology and pathophysiology of schizophrenia. In particular, it has been demonstrated that MK-801, a highly potent and selective NMDA antagonist, induces spatial memory and learning impairments in rodents similar to cognitive deficits observed in patients with schizophrenia. Additionally, it has been shown that MK-801 leads to decreased blood perfusion in brain regions associated with the memory and learning network (i.e., the septohippocampal network). However, there is still a lack of functional connectivity analysis for the impact of MK801 on the septohippocampal network related to learning and memory. Here we conduct a functional connectivity analysis for MK801 effect on the septohippocampal networks using functional Ultrasound Imaging (fUSI) between two groups of mice injected with saline (control) and MK-801. Additionally, we demonstrate the importance of prewhitening fUSI extracted data to eliminate autocorrelation. Results show that prewhitening the data reveals that functional connectivity of certain regions significantly decreases overtime due to the MK-801 effect.

ACKNOWLEDGMENTS

To my PI, Dr. Vasileios Christopoulos, thank you for introducing me to the world of research. You believed in me when I just started, from zero. Words cannot explain the appreciation I have for every second you have dedicated to me in and outside of research.

To my lab fellow colleagues, Dr. Kofi Agyeman and Shan Zhong, thank you for always answering my most simple questions. I have become the researcher I am today by observing you.

To Dr. Edward Ham, you are the one who made me realize my love of science and math, even though I thought I hated them for the longest time. It was not the subjects I disliked; it was the way they were taught in schools. I cannot imagine what would have happened if I never took your class.

To my loving family, your unwavering support and encouragement have been the driving force behind my success. Mom and Dad, your sacrifices, guidance, and unconditional love have shaped me into the person I am today. Your belief in me has given me the strength to pursue my dreams and overcome any obstacle. I am forever grateful for the values you have instilled in me and for always being my rock.

TABLE OF CONTENTS

INTRODUCTION

The N-methyl-D-aspartate receptor (NMDAR) hypofunction hypothesis has been proposed as a potential mechanism underlying the cognitive deficits observed in schizophrenia (Gilmour et al., 2012). This hypothesis suggests that a reduction in NMDAR function may contribute to the pathophysiology of the disorder, particularly in relation to impairments in learning, memory, and executive function (Alherz et al., 2017). To investigate this hypothesis, researchers have utilized pharmacological agents that antagonize NMDAR function, such as dizocilpine (MK-801) (Lee & Zhou, 2019).

MK-801 is a highly potent and selective non-competitive NMDAR antagonist that has been widely used in animal models to induce cognitive deficits similar to those observed in schizophrenia (Blot et al., 2013). Numerous studies have demonstrated that MK-801 administration in rodents leads to impairments in spatial learning and memory, as well as deficits in working memory and cognitive flexibility (Bygrave et al., 2016). These cognitive deficits are thought to arise from the disruption of NMDAR-dependent synaptic plasticity and the consequent alterations in neural network function (Holahan et al., 2011).

The septo-hippocampal network, which comprises the hippocampus and the septum, is a critical neural circuit involved in learning, memory, and spatial navigation (Solari & Hangya, 2018). The hippocampus, in particular, is known to play a crucial role in the formation and consolidation of declarative memories (Huijgen & Samson, 2015). NMDAR-dependent synaptic plasticity within the hippocampus, such as long-term potentiation (LTP), is considered a fundamental mechanism underlying learning and memory processes (Hunt & Castillo, 2012). Disruption of NMDAR

function within the septo-hippocampal network has been implicated in the cognitive deficits associated with schizophrenia and other neuropsychiatric disorders (Peer et al., 2017).

Previous studies have shown that MK-801 administration leads to a reduction in cerebral blood flow and glucose metabolism within brain regions associated with the septo-hippocampal network (Nehls et al., 1990). These findings suggest that NMDAR hypofunction may result in altered neural activity and metabolic dysfunction within this critical circuit. However, the specific impact of MK-801 on functional connectivity within the septo-hippocampal network and its relation to cognitive deficits remains poorly understood.

Functional ultrasound imaging (fUSI) is a novel neuroimaging technique that allows for the high-resolution mapping of cerebral blood volume (CBV) changes with excellent spatial and temporal resolution. fUSI has emerged as a powerful tool for investigating dynamic changes in brain activity and functional connectivity in animal models (Urban et al., 2015). By measuring CBV changes as a proxy for neural activity, fUSI enables the assessment of functional connectivity between brain regions and how it is altered in response to pharmacological interventions or disease states (Crown et al., 2024).

In the present study, we aimed to investigate the effects of MK-801 administration on functional connectivity within the septo-hippocampal network and its adjacent regions using fUSI in a mouse model. We hypothesized that MK-801 would lead to a reduction in functional connectivity within this network, reflecting the disruption of NMDAR-dependent signaling and its impact on neural circuit function. Furthermore, we sought to address the potential confounding effects of autocorrelation in fUSI data by employing a prewhitening procedure using an autoregressive integrated moving average (ARIMA) model. By comparing the results

obtained from raw and prewhitened data, we aimed to provide a more accurate assessment of the temporal dynamics of functional connectivity changes induced by MK-801.

The findings of this study may provide valuable insights into the mechanisms underlying cognitive deficits in schizophrenia and other neuropsychiatric disorders associated with NMDAR hypofunction. Understanding the impact of MK-801 on functional connectivity within the septo-hippocampal network may inform the development of novel therapeutic strategies targeting this critical circuit. Moreover, this study highlights the importance of accounting for autocorrelation in fUSI data analysis to ensure the reliability and validity of functional connectivity measures.

METHODS

2.1. Animal acquisition & Surgical Procedures

Sixteen male C57BL/6 mice, aged between 8 and 12 weeks, were procured from Charles River Laboratories (Hollister, CA). stratified into two principal experimental cohorts: a vehicle control group receiving saline administration (n = 8), and a treatment group receiving the pharmacological agent MK-801 (n = 8).

Prior to experimental procedures, the mice were anesthetized via inhalation of 5% isoflurane, delivered in a carrier gas mixture comprised of oxygen and nitrous oxide in a 1:2 ratio. Subsequently, the anesthetic depth was maintained at a constant rate, ranging from 1.5% to 2%, throughout the surgical intervention and data acquisition phases. Thermoregulatory measures were implemented to maintain physiological body temperature during the recording sessions, achieved by positioning the subjects on an electric heating pad. Furthermore, to facilitate unobstructed transcranial imaging, the hair on the cranial region of each mouse was removed using a commercially available depilatory cream (Nair, Pharmapacks). All procedures were approved by the University of Southern California, Institutional Animal Care and Use Committee (IACUC #21006)

2.2 Data Acquisition

fUSI data were obtained employing the Iconeus One system (Iconeus, Paris, France). Image acquisition was facilitated by a linear ultrasound transducer (i.e., fUSI probe) array comprising 128 channels, operating at a center frequency of 15 MHz with a pitch of 0.1 mm. This methodology afforded a comprehensive field of view, encompassing a width of 12.8 mm, a depth of 10 mm, and a plane thickness of 400 μm. Furthermore, the technique resulted in a spatial

resolution of 100 μm x 100 μm within the imaging plane. The ultrasound transducer was positioned on the intact skull and cutaneous tissue along the sagittal plane of the right cerebral hemisphere. Continuous functional ultrasound imaging (fUSI) data were acquired for a duration of 60 minutes, with the imaging plane oriented sagittal to facilitate imaging of the septohippocampal network within the right hemisphere. 40 minutes of this data were used for data analysis. This decision was informed by previous studies where the dose of MK-801 in the brain was seen to peak systematically approximately 40-60 min post injection (Wegener et al. 2011). Prior to recording, a butterfly needle was inserted to minimize the potential for motion artifacts arising from the subsequent injection procedure. Following an initial 5-minute baseline recording period, an intraperitoneal (i.p.) injection was administered, with the subjects receiving either 0.2 cc of saline solution (vehicle control group) or MK-801 at a dosage of 1.5 mg/kg (treatment group). This dosage was chosen according to previous studies which have established that a 1.0 mg/kg MK-801 injection elicits behavioral and physiological symptoms analogous to those observed in schizophrenia (Long et al. 2006).

2.3 Plane Selection & Imaging

The image acquisition plane of interest was identified through the co-registration of a three-dimensional whole-brain functional ultrasound imaging (fUSI) dataset for each individual mouse with a standardized Allen Mouse Common Coordinates Framework brain atlas. This process was facilitated by dedicated software integrated within the Iconeus One system. To maintain a consistent field of view (FOV) throughout the experimental procedures, the ultrasound probe was securely mounted on a motorized system, with the transverse FOV intersecting the previously co-registered sagittal imaging plane. The imaging data were acquired through the compounding of 200 frames, captured at a frame rate of 500 Hz. This process employed 11 tilted

plane waves, incrementally separated by 2 degrees, spanning from -10° to +10°. The acquisition sequence was executed at a pulse repetition frequency (PRF) of 5.5 kHz, employing real-time continuous acquisition of successive blocks. Each block consisted of 400 ms of compounded plane wave images, followed by a 600 ms pause between pulses.

2.4 Data Pre-processing

pD images generated by the Iconeus One acquisition system undergo pre-processing through the application of integrated algorithms. These built-in algorithms employ singular value decomposition (SVD) techniques for clutter filtering (Ledoux et al. 1997), as well as phase correlation methods for sub-pixel motion registration. To derive the pD images, the algorithms were utilized to isolate the blood signal from the tissue signal. Potential physiological and motion artifacts were addressed through the adoption of rigid motion correction techniques, which have proven effective in functional ultrasound imaging (fUSI) and other neuroimaging modalities (Stringer et al. 2019). These motion correction measures were integrated with high-frequency filtering algorithms to suppress noise-related artifacts. Specifically, a low-pass filter with a normalized passband frequency of 0.02 Hz and a stopband attenuation of 60 dB was implemented. This filter incorporated a delay compensation mechanism to mitigate any temporal distortions introduced by the filtering process itself, thereby facilitating the effective removal of high-frequency fluctuations from the pD signal data.

2.5 Statistical Analysis Tools

All analysis was performed on MATLAB 9.12.0.1927505 (R2022a) to 24.1.0.2537033 (R2024). For FC analysis of intraperitoneally administered MK-801 on the within septohippocampal network and its adjacent areas, we first calculated the percent change in cerebral blood volume

(ΔCBV) relative to baseline measurements (i.e., the average ΔCBV of first 5 min prior to saline or MK-801 injection) for the time series of each region of interest (ROI). To investigate the temporal dynamics of FC within the network, we employed a rolling functional connectivity (RFC) approach. This method involves calculating the Pearson correlation coefficient *r* of a pair of time series using a sliding window of 60 seconds, which was applied throughout the entire duration of the recording (2400 seconds). This enabled us to capture the evolution of functional connectivity over time.

$$r = \frac{\Sigma(x_i - \underline{x})(y_i - \underline{y})}{\sqrt{\Sigma(x_i - \underline{x})^2 (y_i - \underline{y})^2}}$$

To quantify these temporal evolutions, we fit a linear model to the RFC and use the slopes of the regression model for each ROI pair RFC to evaluate change of FC overtime and conduct a two-sided significance test about each slope against the mean of 0 ($p < 0.05$). We validate the assumptions of the regression model by assessing normality through histograms (Figure 1.c) and QQ-plots of the residuals (Figure 1.d). According to the histograms and QQ-plots, the residual plots for all RFCs were deemed to be approximately normally distributed, confirming the suitability of employing linear regression.

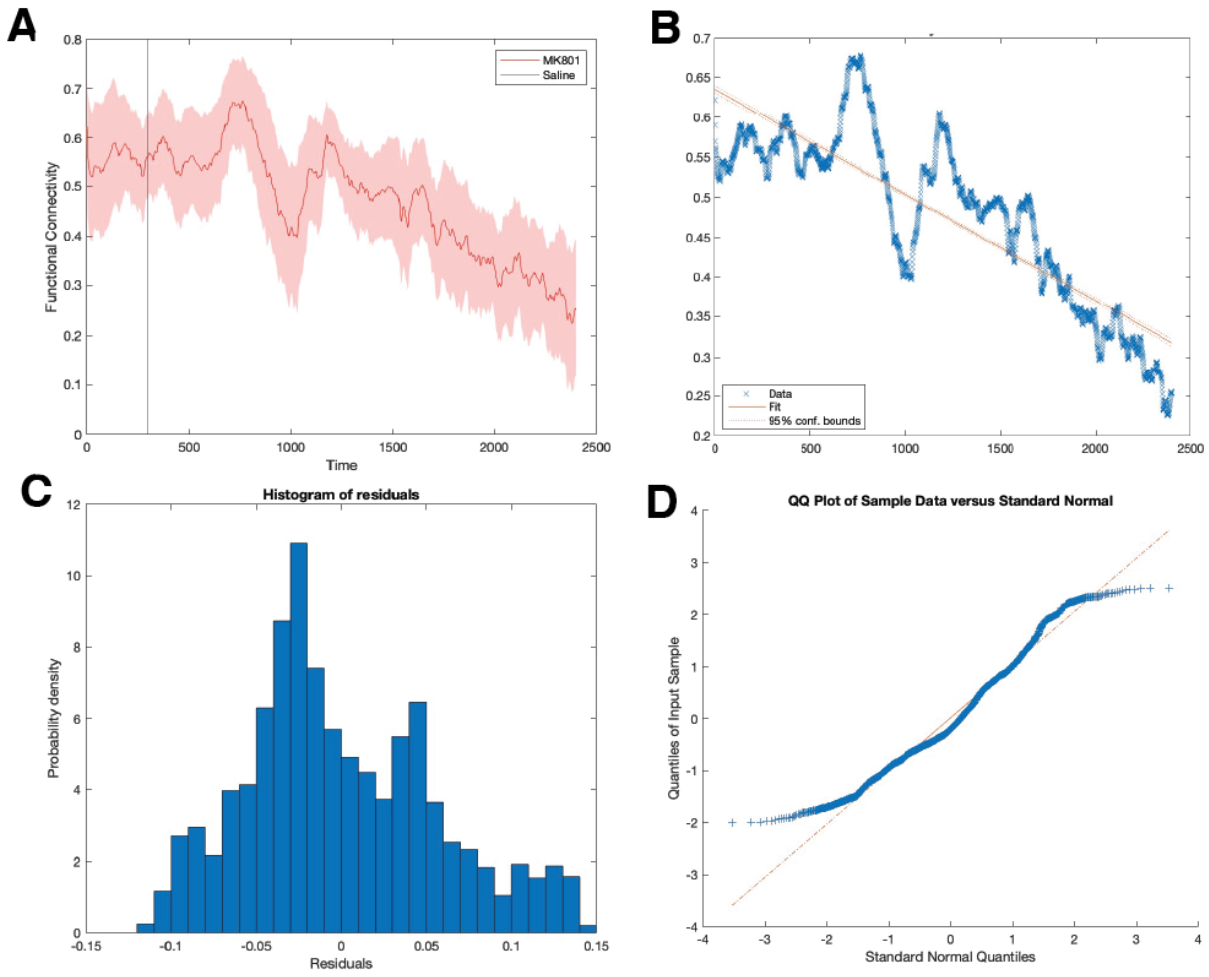

Figure 1. Assessment of the linear regression model used to quantify temporal changes in functional connectivity.
(A) Representative example of a rolling functional connectivity (RFC) plot between Hippocampus and Striatum in MK-801 group the shaded areas representing 95% confidence intervals. The linear regression model is fitted to the RFC data to obtain the slope, which represents the rate of change in functional connectivity over time.
(B) Plot of calculated linear slope alongside the RFC points from part (A), highlighting the fitted regression lines for both groups. The shaded areas represent the 95% confidence bounds for each regression line.
(C) Histogram of the residuals obtained from the linear regression model, demonstrating the approximately normal distribution of the residuals.
(D) Quantile-Quantile (QQ) plot of the residuals against the standard normal distribution. The close alignment of the residuals to the diagonal line further confirms the normality assumption of the linear regression model. The normality of the residuals, as assessed by the histogram and QQ plot, validates the use of linear regression for analyzing the temporal changes in functional connectivity.

2.6 Prewhitening

The motion-corrected power Doppler time series data from the 6 ROIs subsequent exhibited non-stationarity with strong autocorrelation according to the AutoCorrelation Function (ACF) and Partial AutoCorrelation Function (PACF) plots (fig 3a). This is typically expected from biological systems including the brain (Derado et al. 2010). Thus, one of the steps was to conduct FC analysis on prewhitened (PW) data, which is the data that is void of autocorrelation, and compare it with the non-PW counterpart. We accomplished this by employing a predictive modeling approach based on the **A**uto**R**egressive **I**ntegrated **M**oving **A**verage (ARIMA) framework pioneered by Box and Gen (Box et al. 2015). This mathematical model is the combination of an autoregressive model, integration of data and moving average models with which respectively are represented in degrees of *(p, d, q)*. By fine tuning these parameters we can facilitate the forecasting of a future time point y_t by explicitly incorporating the contributions of autocorrelation from its preceding values, namely $\{y_{t-n}, \ldots, y_{t-2}, y_{t-1}\}$. Upon obtaining the forecasted time series y_t, which is informed by the autocorrelative structure of the data, we can proceed to calculate the residuals ε_t by subtracting y_t from the original time series, where ω represents a constant.

$$y_t = \omega + \phi y_{t-p} + \varepsilon_t$$

Prewhitened series:

$$\boldsymbol{\varepsilon_t = y_t - \omega + \phi y_{t-p}} \quad (1)$$

This operation yields a residual sequence (ε_t) that is characterized by the absence of autocorrelation, commonly referred to as "white noise". This process, known as **prewhitening**, effectively removes the temporal dependencies inherent in the original data.

Before diving into prewhitening, we must understand that in a time series data, correlation comes in two forms as shown below: Direct, and Indirect. In prewhitening data it's important to take both of these types of correlations into account. A great tool for inspecting these two correlations is the ACF and the PACF as they plot distinct types of correlations as a function of lag of the time series. Here, a "lag" of a time series y, denoted by $L^n\{y\}$,simply refers to shifting the time series by a specific number of time periods. For example, a lag of 1 means shifting the entire time series data forward by 1 time period. Thus, the correlation of lag 0 will be the correlation of the time series with itself, yielding a value of 1. The difference between ACF and PACF is in the inclusion of indirect correlation. The ACF estimates the Pearson correlation coefficient between a timepoint y_t and its lagged counterpart y_{t-n}, thereby incorporating both direct and indirect dependencies. In contrast, the PACF computes the correlation between y_t and y_{t-n} while controlling for the intervening correlations between y_{t-1} to y_{t-n-1}, thus isolating the direct dependence at $L^n\{y\}$. Thus, by continually plotting the ACF and PACF of our modified time series throughout our analysis we can understand how much of the direct and indirect correlation we have eliminated from our original data. Throughout our prewhitening procedure, ACF and PACF will serve as a visualization tool to understand how much of the correlation we have eliminated from our original time series.

2.6.1 Integration (d)

In time series data, we do not have independence as the measurement of some time period depends on the measurement of that value on the previous time periods. But to build predictive models, we need consistency, specifically within distributions. As ARIMA is a stationary class model, its first assumption is that the underlying time series is stationary. A time series is deemed stationary if it meets the following three criteria (Saridakis & Papaioannou, 2014):

1. The mean (μ) is constant, typically assumed to be zero.
2. The variance (σ) is constant across all time intervals of t.
3. There is no seasonality within the time series

This underlying assumption is crucial as in a non-stationary time series, the relationships between observations and their dependence on past values can change over time. This violates the assumption of constant statistical properties, making it difficult to capture and model the underlying patterns accurately. Stationarity ensures that the relationships and dependencies within the data remain consistent, allowing the model to reliably capture and exploit these patterns. We can check for the 3 stationary criteria by simply plotting and visually analyzing the time series. For example, figure 2a depicts the hippocampal time series data from a representative MK mouse, illustrating the oscillatory patterns exhibited by this brain region. We observe an overall time trend and inconsistent variation throughout the time series. We remove this trend by differentiating the time series. Differencing is the process of computing the difference between consecutive observations in a time series to remove trends or seasonality. Notably, the 'integrated' component of the ARIMA model corresponds to the degree of differencing, represented by the parameter d in the conventional ARIMA (p, d, q) notation. This

parameter tells us the number of times the differencing operation needs to be applied to make the time series stationary.

$$y_t = \omega + y_{t-1} + \varepsilon_t$$

Differencing: $y_t - y_{t-1} = \omega + \varepsilon_t$

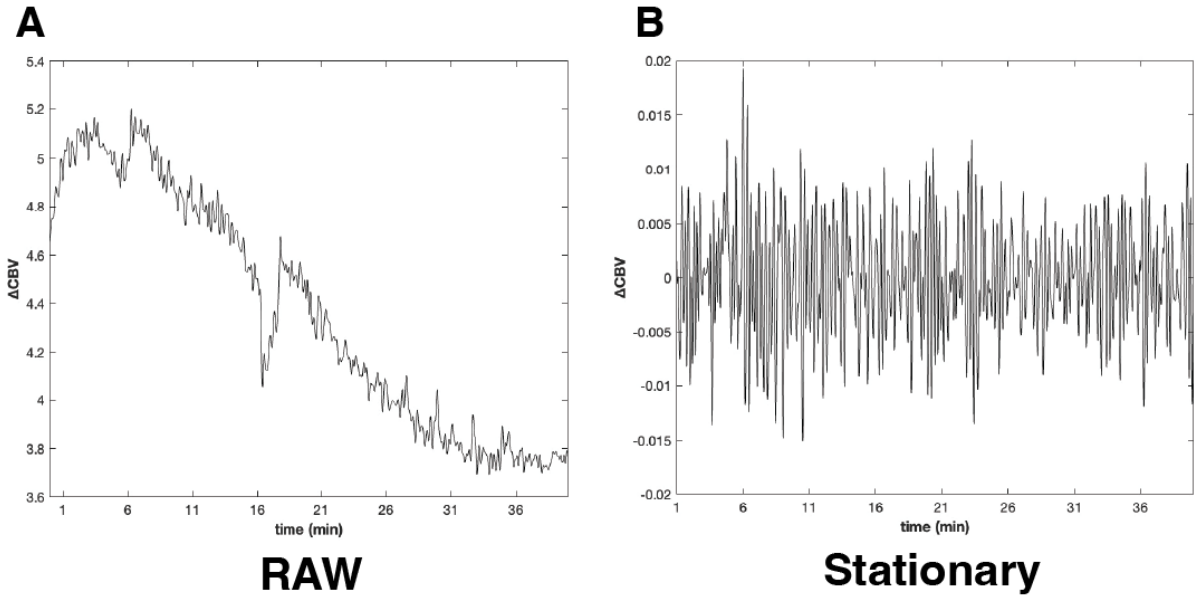

Figure 2. Transformation of non-stationary hippocampal CBV time series data into a stationary process using differencing.
(A) Raw hippocampal CBV time series data from a representative MK-801-treated mouse, exhibiting non-stationary oscillatory patterns with an overall time trend and inconsistent variation throughout the series.
(B) Differenced (ARIMA (0, 1, 0)) hippocampal CBV time series data, demonstrating a stationary process with a constant mean ($\mu = 0$) and constant variance across the series. The differencing procedure removes the time trend and stabilizes the variance, resulting in a series characterized by white noise (ε_t) with constant statistical properties.

By simply taking the first difference or ARIMA (0, 1, 0) of our non-stationary time series, we are left with $\omega + \varepsilon_t$. ω represents a constant and ε_t is just white noise with constant mean and variance. Thus, since they both have constant statistical properties (i.e., mean, variance), we are

left with a stationary time series. By doing this procedure with fig## left panel, we obtain the right panel which shows us the differenced time series. By visual observation, we see that the differenced time series has a constant $mean, \mu = 0$ and a constant variance across the series. We further observe this by performing the Augmented Dickey-Fuller test for stationarity. As we are confident in the stationarity of the time-series, we can move on to the model building process

2.6.2 AutoRegressive (AR)

As previously mentioned, the ARIMA model forecasting capability relies on the incorporation of historical time points. In time series, each datapoint is dependent on the previous one, thus the AR part of ARIMA is essentially based solely on historical values of that series called Lags. Thus, by building a regression model of the form

$$
\begin{aligned}
&AR(1): \quad y_t = \omega + \phi_1 y_{t-1} + \varepsilon_t \\
&AR\ (2): \quad y_t = \omega + \phi_1 y_{t-1} + \phi_2 y_{t-2} + \varepsilon_t \\
&AR(p): \quad y_t = \omega + \phi_1 y_{t-1} + \phi_2 y_{t-2} + \ldots + \phi_p y_{t-p} + \varepsilon_t
\end{aligned} \tag{1}
$$

where ω is the constant, ε_t the white noise, and $\{\phi_1 y_{t-1} + \phi_2 y_{t-2} + \ldots + \phi_p y_{t-p}\}$ is the previous time points or lags, we can predict the future time point y_t based on the inherent dynamics of the series.

2.6.3. Moving Average (MA)

Thus the MA model depends not on the previous values of Y but the previous errors, i.e., the lagged errors, that exist across time.

$$
\begin{aligned}
&MA(1): \quad y_t = \omega + \phi' \varepsilon_{t-1} + \varepsilon_t \\
&MA(2): \quad y_t = \omega + \phi' \varepsilon_{t-1} + \phi' \varepsilon_{t-2} + \varepsilon_t \\
&MA(q): \quad y_t = \omega + \phi' \varepsilon_{t-1} + \phi' \varepsilon_{t-2} + \ldots + \phi' \varepsilon_{t-q} + \varepsilon_t
\end{aligned} \tag{2}
$$

Where again y_t is the predicted time point, w is the constant, the

$\{\phi\varepsilon_{t-1} + \phi\varepsilon_{t-2} + \ldots + \phi\varepsilon_{t-q}\}$ is the previous time point and e_t is the current error.

2.6.4. ARIMA

Now, by combining the AR model (eq.1) and the MA model (eq.2) we get the equation for the ARIMA model which is:

$$y_t = \omega + \phi_1 y_{t-1} + \ldots + \phi_p y_{t-p} + \phi'\varepsilon_{t-1} + \ldots + \phi'\varepsilon_{t-q} + \varepsilon_t$$

The ARIMA model incorporates both the autoregressive and moving average components, allowing for a more comprehensive representation of the time series dynamics. To determine the optimal ARIMA model for our hippocampal CBV time series data, we employed a systematic approach. We first examined the ACF and partial autocorrelation function (PACF) of the differenced time series to identify potential autoregressive and moving average terms. Based on the ACF and PACF plots, we considered several candidate models and evaluated their goodness of fit using the Akaike Information Criterion (AIC) and Bayesian Information Criterion (BIC). These criteria balance the model's complexity and its ability to explain the data, with lower values indicating a better fit. After comparing various ARIMA models, we found that the ARIMA (4, 1, 0) model provided the best fit for our hippocampal CBV time series data. This model suggests that the current value of the time series depends on the four previous values (autoregressive term of order 4) and that the data has been differenced once to achieve stationarity (differencing term of order 1). The absence of a moving average term (q = 0) indicates that the model does not incorporate lagged forecast errors. To assess the effectiveness of the ARIMA (4, 1, 0) model in removing autocorrelation from the time series data, we examined the ACF and PACF plots of the prewhitened data (Figure 3). As evident in Figure 3B,

the ACF and PACF of the prewhitened data exhibit a dramatic reduction in autocorrelation compared to the raw data (Figure 3A). The majority of the lags in the prewhitened data fall within the shaded confidence interval, suggesting that the residuals are approximately independently distributed. This indicates that the ARIMA (4, 1, 0) model successfully captures and removes the temporal dependencies present in the raw hippocampal CBV time series data, resulting in a more stationary and uncorrelated process. The removal of autocorrelation is crucial for subsequent analyses, as it ensures that the statistical properties of the data are stable over time and that the observations are independent, allowing for valid inference and hypothesis testing.

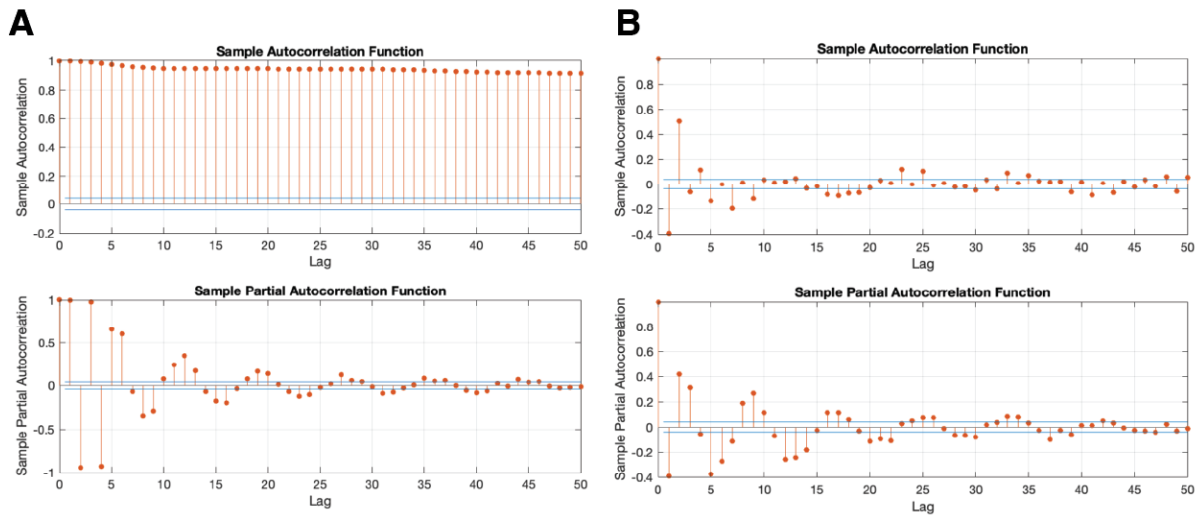

Figure 3. Autocorrelation and partial autocorrelation analysis of raw and prewhitened hippocampal CBV time series data from a representative MK-801-treated mouse.
(A) ACF and PACF of the raw hippocampal CBV time series data. The ACF and PACF plots demonstrate significant autocorrelation across multiple lags, indicating the presence of strong temporal dependencies in the non-prewhitened data.
(B) Sample ACF and sample PACF of the prewhitened hippocampal CBV time series data. After applying the prewhitening procedure, the ACF and PACF plots exhibit a dramatic reduction in autocorrelation, with the majority of the lags falling within the shaded confidence interval. This

suggests that the prewhitened time series more closely resembles an independently distributed process, effectively mitigating the confounding effects of autocorrelation present in the raw data.

RESULTS

3.1 Rolling Functional Connectivity Analysis

To investigate the effects of MK-801 on functional connectivity, we employed a rolling functional connectivity (RFC) analysis. This approach involved calculating the Pearson correlation coefficient between pairs of ROIs using a sliding window technique. For each pair of the 6 ROIs (hippocampus, striatum, pallidum, thalamus, hypothalamus, and mPFC), we first normalized their time series to the initial 5-minute baseline period. We then defined a 60-second window and computed the correlation coefficient between the corresponding segments of the two ROIs' time series. The window was sequentially shifted forward in time until it reached the end of the 2400-second recording period. This process was repeated for all possible pairwise combinations of the 6 ROIs. Figure 4a illustrates an example of RFC calculation process for two representative ROIs (i.e., Hippocampus and Striatum), demonstrating how the correlation coefficient is obtained for each 60-second window and how the window is incrementally moved along the normalized time series until the entire recording duration is covered.

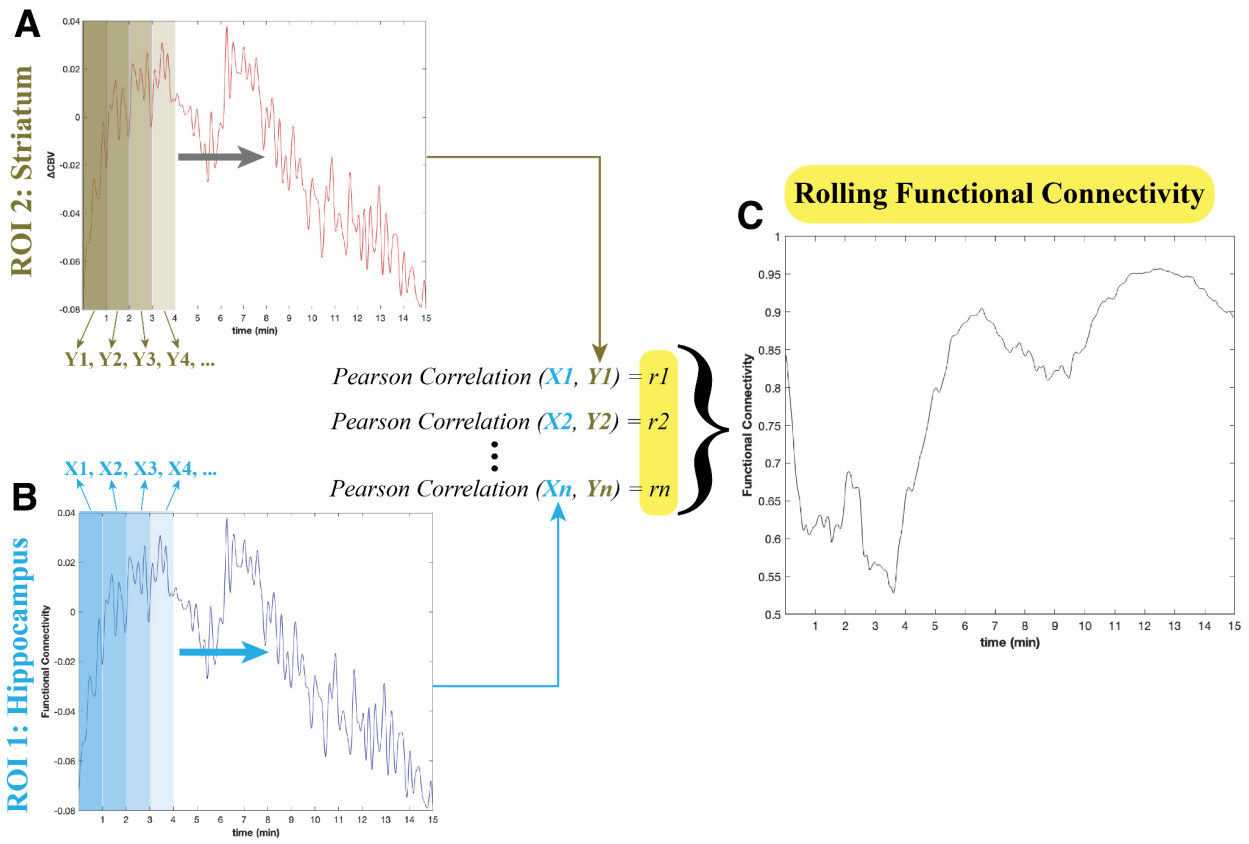

Figure 4. Schematic representation of the rolling functional connectivity (RFC) analysis procedure using time series data from two regions of interest (ROIs) in a representative mouse. **(A)** CBV change over time in the hippocampus (ROI 1). The shaded rectangles $\{Y_1, Y_2, Y_3, \ldots, Y_n\}$ represent the 60-second sliding windows that sequentially move from the beginning to the end of the time series.
(B) CBV changes over time in the striatum (ROI 2). The shaded rectangles $\{X_1, X_2, X_3, \ldots, X_n\}$ represent the corresponding 60-second sliding windows for the striatum time series. For each pair of corresponding windows from the hippocampus and striatum time series, the Pearson correlation coefficient is calculated (e.g., Pearson Correlation $(X_1, Y_1) = r_1$, Pearson Correlation $(X_2, Y_2) = r_2$, ..., Pearson Correlation $(X_n, Y_n) = r_n$). **(C)** The resulting rolling functional connectivity plot, obtained by plotting the calculated Pearson correlation coefficients $(r_1, r_2, \ldots, r_n)$ against the time points corresponding to each window pair. This RFC procedure enables the assessment of dynamic changes in functional connectivity between the two ROIs throughout the recorded period.

By employing this RFC analysis, we captured the dynamic changes in functional connectivity between brain regions over the experiment. Afterwards, we applied linear regression analysis to

quantify the temporal changes in functional connectivity. By fitting a linear regression model to each pairwise RFC plot, we obtained the slopes of the regression lines, which represent the approximate rate of change in functional connectivity over time. The resulting slopes were extracted for both the saline and MK-801 groups and plotted on a connectivity matrix (Figure 6a). Comparing the slope connectivity matrix of both groups, we found that the MK-801 group (right panel) exhibited a more pronounced decrease in FC over time. This was evident from the fact that a larger number of ROI pairs in the MK-801 group showed a significant decrease in correlation compared to the saline group (left panel).

3.2 Effect of Autocorrelation Removal

The effectiveness of the ARIMA (4, 1, 0) model in reducing autocorrelation is clearly illustrated in Figure 3b. The ACF and PACF plots of the raw ΔCBV time series (left panels) show significant autocorrelation across multiple lags, indicating the presence of strong temporal dependencies in the data. In contrast, after applying the pseudo-prewhitening procedure (right panels), the ACF and PACF plots exhibit a dramatic reduction in autocorrelation. The majority of the lags fall within the shaded confidence interval, suggesting that the prewhitened time series are much closer to being independently distributed.

After prewhitening, we calculated the linear regression slopes on the RFC of the pseudo-PW time series (Figure 5b) and compared the resulting connectivity matrices to those obtained from the raw (i.e., non-PW) data. The comparison revealed striking differences in the patterns of significant slopes between the two preprocessing approaches. In the MK-801 group, the

prewhitened data (Figure 5b; right panel), showed a significant decrease in functional connectivity across all pairwise ROIs, suggesting a widespread reduction in the temporal dynamics of functional connectivity induced by MK-801. This finding contrasts with the more localized changes observed in the raw data, where significant decreases were primarily concentrated in the functional connectivity between the hippocampus and other ROIs. Looking at the heatmap intensity of the slopes in the MK-801 group prewhitened data (Figure 5b; right panel), the largest decreases were observed primarily in the functional connectivity between the hippocampus and the other 5 ROIs. This finding highlights the particularly strong impact of MK-801 on the temporal dynamics of hippocampal functional connectivity, which is consistent with the role of NMDA receptors in hippocampal-dependent learning and memory processes.

On the other hand, the prewhitened saline group (Figure 5b; left panel) exhibited a notable shift in the distribution of significant slopes after prewhitening. While the raw data indicated significant changes mostly in the FC between the striatum and other ROIs, the prewhitened data revealed a more diverse pattern of significant slopes. These significant slopes were now mostly distributed among individual connections of both the mPFC and thalamus with the striatum and pallidum. This suggests that the prewhitening procedure uncovered additional temporal dynamics in the saline group that were previously obscured by autocorrelation in the raw data.

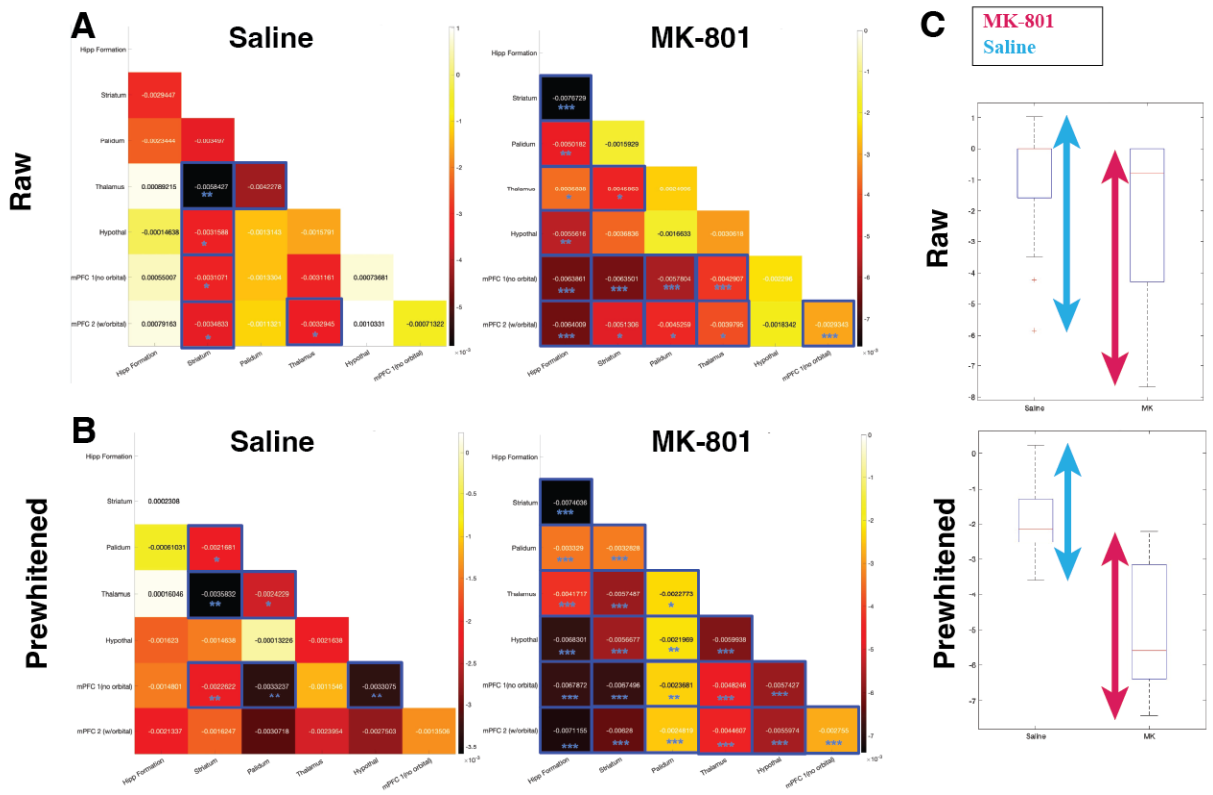

Figure 5. Comparison of functional connectivity changes over time between saline and MK-801 groups using linear regression slopes derived from rolling functional connectivity (RFC) analysis.

(A) Connectivity matrices displaying the slopes of linear regression lines fitted to the RFC plots for each pair of regions of interest (ROIs) in the saline (left panel) and MK-801 (right panel) groups using raw (non-prewhitened) data. The MK-801 group exhibits a more pronounced decrease in functional connectivity over time, as evident from the larger number of significantly negative slopes compared to the saline group.

(B) Connectivity matrices displaying the slopes of linear regression lines fitted to the RFC plots for each ROI pair in the saline (left panel) and MK-801 (right panel) groups using prewhitened data. Prewhitening reveals a widespread reduction in the temporal dynamics of functional connectivity induced by MK-801, with the largest decreases observed primarily between the hippocampus and other ROIs. In contrast, the prewhitened saline group shows a more diverse pattern of significant slopes, with changes mostly distributed among connections of the mPFC and thalamus with the striatum and pallidum.

(C) Distribution of averaged slopes from the connectivity matrices for saline and MK-801 groups using raw (upper panel) and prewhitened (bottom panel) data. The substantial overlap between the distributions in the raw data indicates no significant difference in temporal effects on functional connectivity between the groups. However, after prewhitening, the slope distributions become more separated, suggesting a distinct and pronounced effect of MK-801 on

functional connectivity over time compared to the saline control. (Asterisks indicate the level of significance: * $p < 0.05$, ** $p < 0.01$, *** $p < 0.001$)

3.3 Comparison of Temporal Effects on Functional Connectivity Between Saline and MK-801 Groups

As a final step in our analysis, we aimed to compare the extent of the decrease in functional connectivity over time between the saline and MK-801 groups, to determine which condition had a more pronounced effect on the temporal dynamics of functional connectivity. We plotted the distribution of all the averaged slopes shown in the connectivity matrices for both saline and MK-801, using both raw and prewhitened data (Figure 5c). In the non-prewhitened slopes (upper panel), we observed a substantial overlap between the distributions, indicating no significant difference in the temporal effects on functional connectivity between the saline and MK-801 groups. However, after prewhitening (bottom panel), the plotted slope distributions for the saline and MK-801 groups became much more separated, with minimal overlap. This clear separation suggests that the effect of MK-801 on functional connectivity over time was much more distinct and pronounced compared to the control (saline) condition after removing the confounding influence of autocorrelation. The prewhitening process revealed the true temporal impact of MK-801 on functional connectivity, which was previously obscured by the presence of autocorrelation in the raw data. This finding underscores the importance of accounting for autocorrelation when investigating the temporal dynamics of functional connectivity, particularly in the context of pharmacological interventions such as MK-801 administration.

DISCUSSION

4.1 Declining FC Over Time with MK-801

The present study aimed to investigate the effects of the NMDA receptor antagonist MK-801 on dynamic functional connectivity within the septo-hippocampal network and its adjacent areas using fUSI. To explore the temporal dynamics of functional connectivity, we employed a rolling RFC analysis. This approach revealed that MK-801 administration not only affects the overall strength of functional connectivity but also leads to a more rapid decline in connectivity between brain regions involved in learning and memory over time. Specifically, the MK-801 group exhibited a more pronounced decrease in functional connectivity when prewhitened across all pairwise ROIs compared to the saline group (Telesford et al., 2016).

4.2 The Impact of Autocorrelation Removal on fUSI Data

Importantly, our study highlights the crucial role of accounting for autocorrelation when analyzing time series data. By applying a pseudo-prewhitening procedure using an ARIMA (4, 1, 0) model, we were able to remove the confounding effects of autocorrelation. The stark difference observed between the raw and prewhitened data underscores the importance of this step, as failing to account for autocorrelation could lead to biased or spurious results in subsequent analyses (Schaffer, Dobbins, & Pearson, 2021). The prewhitened data revealed a particularly strong impact of MK-801 on the temporal dynamics of hippocampal functional connectivity. The pronounced reduction in the slopes of hippocampal functional connectivity suggests that MK-801 administration not only disrupts the overall strength of connections but also leads to a more rapid decline in the temporal dynamics of functional interactions between the hippocampus and other key regions involved in cognitive processing. This finding is

consistent with the critical role of NMDA receptors in hippocampal-dependent learning and memory processes (Brigman et al., 2010).

4.3 Implications and Future Directions

The findings of this study have important implications for understanding the mechanisms underlying learning and memory related deficits observed in neuropsychiatric disorders such as schizophrenia (Lee et al., 2020). By demonstrating the impact of NMDA receptor hypofunction on functional connectivity within and outside of the septo-hippocampal network, our results provide valuable insights into the potential neural substrates of cognitive impairments associated with these disorders. Future studies should aim to further elucidate the specific mechanisms by which MK-801 disrupts functional connectivity and explore potential therapeutic interventions that target these mechanisms. Additionally, investigating the effects of MK-801 on functional connectivity in awake, behaving animals could provide a more comprehensive understanding of how NMDA receptor hypofunction impacts cognitive processes in real-time.

4.4 Limitations

It is important to acknowledge the limitations of the current study. First, the sample size was relatively small, and future studies with larger cohorts may provide more robust and generalizable findings. Second, the use of anesthetized animals may have caused changes in the CBV (Masamoto & Kanno, 2012), and future studies in awake animals could help mitigate this potential confound. Lastly, while fUSI provides high spatial and temporal resolution, it is limited to a single imaging plane, and future studies employing multi-plane or three-dimensional

imaging techniques could offer a more comprehensive view of the brain-wide effects of MK-801 (Rabut et al., 2019)

In conclusion, our study demonstrates that MK-801 administration leads to a more rapid decline in functional connectivity as a function of time within and outside the septo-hippocampal network. These findings underscore the importance of NMDA receptor signaling in maintaining normal functional connectivity and provide valuable insights into the potential neural mechanisms underlying cognitive deficits observed in neuropsychiatric disorders. Furthermore, our results highlight the critical importance of accounting for autocorrelation when analyzing time series data to ensure accurate and reliable conclusions.

REFERENCES

Gilmour, G., Dix, S., Fellini, L., Gastambide, F., Plath, N., Steckler, T., Talpos, J., & Tricklebank, M. (2012). NMDA receptors, cognition and schizophrenia – Testing the validity of the NMDA receptor hypofunction hypothesis. Neuropharmacology, 62, 1401-1412. https://doi.org/10.1016/j.neuropharm.2011.03.015.

Alherz, F., Alherz, M., & Almusawi, H. (2017). NMDAR hypofunction and somatostatin-expressing GABAergic interneurons and receptors: A newly identified correlation and its effects in schizophrenia. Schizophrenia Research: Cognition, 8, 1 - 6. https://doi.org/10.1016/j.scog.2017.02.001.

Lee, G., & Zhou, Y. (2019). NMDAR Hypofunction Animal Models of Schizophrenia. Frontiers in Molecular Neuroscience, 12. https://doi.org/10.3389/fnmol.2019.00185.

Blot, K., Bai, J., & Otani, S. (2013). The effect of non-competitive NMDA receptor antagonist MK-801 on neuronal activity in rodent prefrontal cortex: an animal model for cognitive symptoms of schizophrenia. Journal of Physiology-Paris, 107, 448-451. https://doi.org/10.1016/j.jphysparis.2013.04.003.

Bygrave, A., Masiulis, S., Nicholson, E., Berkemann, M., Barkus, C., Sprengel, R., Harrison, P., Kullmann, D., Bannerman, D., & Kätzel, D. (2016). Knockout of NMDA-receptors from parvalbumin interneurons sensitizes to schizophrenia-related deficits induced by MK-801. Translational Psychiatry, 6. https://doi.org/10.1038/tp.2016.44.

Holahan, M., Madularu, D., McConnell, E., Walsh, R., & DeRosa, M. (2011). Intra-Accumbens Injection of a Dopamine Aptamer Abates MK-801-Induced Cognitive Dysfunction in a Model of Schizophrenia. PLoS ONE, 6. https://doi.org/10.1371/journal.pone.0022239.

Solari, N., & Hangya, B. (2018). Cholinergic modulation of spatial learning, memory and navigation. *The European Journal of Neuroscience*, 48, 2199 - 2230. https://doi.org/10.1111/ejn.14089.

Huijgen, J., & Samson, S. (2015). The hippocampus: A central node in a large-scale brain network for memory. Revue neurologique, 171 3, 204-16. https://doi.org/10.1016/j.neurol.2015.01.557.

Hunt, D. L., & Castillo, P. E. (2012). Synaptic plasticity of NMDA receptors: mechanisms and functional implications. Current opinion in neurobiology, 22(3), 496–508. https://doi.org/10.1016/j.conb.2012.01.007

Peer, M., Prüss, H., Ben-Dayan, I., Paul, F., Arzy, S., & Finke, C. (2017). Functional connectivity of large-scale brain networks in patients with anti-NMDA receptor encephalitis: an observational study. The lancet. Psychiatry, 4 10, 768-774. https://doi.org/10.1016/S2215-0366(17)30330-9.

Nehls, D., Park, C., MacCormack, A., & Mcculloch, J. (1990). The effects of N-methyl-D-aspartate receptor blockade with MK-801 upon the relationship between cerebral blood flow and glucose utilization. Brain Research, 511, 271-279. https://doi.org/10.1016/0006-8993(90)90172-8.

Urban, A., Dussaux, C., Martel, G., Brunner, C., Macé, E., & Montaldo, G. (2015). Real-time imaging of brain activity in freely moving rats using functional ultrasound. Nature Methods, 12, 873-878. https://doi.org/10.1038/nmeth.3482.

Crown, L. M., Agyeman, K. A., Choi, W., Zepeda, N., Iseri, E., Pahlavan, P., Siegel, S. J., Liu, C., Christopoulos, V., & Lee, D. J. (2024). Theta-frequency medial septal nucleus deep

brain stimulation increases neurovascular activity in MK-801-treated mice. Frontiers in neuroscience, 18, 1372315. https://doi.org/10.3389/fnins.2024.1372315

Wegener, N., Nagel, J., Gross, R., Chambon, C., Greco, S., Pietraszek, M., ... & Danysz, W. (2011). Evaluation of brain pharmacokinetics of (+) MK-801 in relation to behaviour. Neuroscience letters, 503(1), 68-72.

Long, L. E., Malone, D. T., & Taylor, D. A. (2006). Cannabidiol reverses MK-801-induced disruption of prepulse inhibition in mice. Neuropsychopharmacology, 31(4), 795-803.

Ledoux, L. A., Brands, P. J., & Hoeks, A. P. (1997). Reduction of the clutter component in Doppler ultrasound signals based on singular value decomposition: A simulation study. Ultrasonic imaging, 19(1), 1-18.

Stringer, C., & Pachitariu, M. (2019). Computational processing of neural recordings from calcium imaging data. Current opinion in neurobiology, 55, 22-31.

Derado, G., Bowman, F. D., Ely, T. D., & Kilts, C. D. (2010). Evaluating Functional Autocorrelation within Spatially Distributed Neural Processing Networks. Statistics and its interface, 3(1), 45–58. https://doi.org/10.4310/sii.2010.v3.n1.a4

Box, G. E., Jenkins, G. M., Reinsel, G. C., & Ljung, G. M. (2015). Time series analysis: forecasting and control. John Wiley & Sons.

Saridakis, G., & Papaioannou, G. (2014). Analysis of Non-Stationary Time-Series Business Data, 96-103. https://doi.org/10.4018/978-1-4666-5202-6.CH010.

Telesford, Q., Lynall, M., Vettel, J., Miller, M., Grafton, S., & Bassett, D. (2016). Detection of functional brain network reconfiguration during task-driven cognitive states. NeuroImage, 142, 198-210. https://doi.org/10.1016/j.neuroimage.2016.05.078.

Schaffer, A., Dobbins, T., & Pearson, S. (2021). Interrupted time series analysis using autoregressive integrated moving average (ARIMA) models: a guide for evaluating large-scale health interventions. BMC Medical Research Methodology, 21. https://doi.org/10.1186/s12874-021-01235-8.

Brigman, J., Wright, T., Talani, G., Prasad-Mulcare, S., Jinde, S., Seabold, G., Mathur, P., Davis, M., Bock, R., Gustin, R., Colbran, R., Alvarez, V., Nakazawa, K., Delpire, E., Lovinger, D., & Holmes, A. (2010). Loss of GluN2B-Containing NMDA Receptors in CA1 Hippocampus and Cortex Impairs Long-Term Depression, Reduces Dendritic Spine Density, and Disrupts Learning. The Journal of Neuroscience, 30, 4590 - 4600. https://doi.org/10.1523/JNEUROSCI.0640-10.2010.

Lee, J., Buuse, M., Nithianantharajah, J., & Jones, N. (2020). Acute NMDA receptor antagonism impairs working memory performance but not attention in rats-Implications for the NMDAr hypofunction theory of schizophrenia. Behavioral neuroscience, 134 4, 323-331. https://doi.org/10.1037/bne0000402.

Masamoto K, Kanno I. Anesthesia and the quantitative evaluation of neurovascular coupling. J Cereb Blood Flow Metab. 2012 Jul;32(7):1233-47. doi: 10.1038/jcbfm.2012.50. Epub 2012 Apr 18. PMID: 22510601; PMCID: PMC3390804.

Rabut, C., Correia, M., Finel, V., Pezet, S., Pernot, M., Deffieux, T., & Tanter, M. (2019). 4D functional ultrasound imaging of whole-brain activity in rodents. Nature methods, 16, 994 - 997. https://doi.org/10.1038/s41592-019-0572-y.